

The fast marching method in Spherical coordinates: SEG/EAGE salt-dome model

Tariq Alkhalifah¹

keywords: *traveltimes, finite difference*

ABSTRACT

Applying the fast marching method to solve the eikonal equation on the 3-D SEG/EAGE salt-dome model demonstrates two key features of the method, stability and efficiency. Such an application, also reveals some of the accuracy deficiencies of the Cartesian-coordinate implementation of the fast marching method. The accuracy is improved by applying the fast marching method in spherical coordinates. Obviously, this domain better represents waves emanating from a point source than the Cartesian coordinates. However, the finite-difference solution of the eikonal equation, in any domain, provides traveltimes corresponding only to the fastest arrivals. These arrivals, in inhomogeneous media, include typically head-waves and other low-energy waves. The eikonal solution of the salt-dome model includes a lot of low energy waves, such as head-waves emanating from the top of the salt structure. These low-energy waves have replaced the more important direct waves in many regions of the solution. Using such a traveltime solution for imaging will result in a less than ideal image.

INTRODUCTION

Sethian (1996) and Sethian and Popovici (1997) recently introduced a method for solving the eikonal equation that they refer to as the *fast marching* method. Their eikonal solver has two very important features: it is unconditionally stable and, at the same time, highly efficient. Their method is based on solving the eikonal equation on a Cartesian grid along the wavefront, starting with those points with minimum traveltime—an idea similar to the method of *expanding wavefronts* (Qin et al., 1992). As a result, a minimum traveltime tree is constructed using fast algorithms (heap sorting) with computational cost proportional to $\log N$, where N is the number of grid points in the computational domain. Therefore, the cost of the eikonal solver is roughly proportional to $N \log N$. By starting traveltime calculation from those points with minimum traveltime, the stability of the algorithm is ensured regardless of the complexity of the velocity model.

¹**email:** tariq@sep.stanford.edu

The impressive features of the fast marching method, stability and efficiency, are achieved at the expense of accuracy. The approach is based on a first-order approximation of the traveltime derivatives with respect to position. This low-order approximation can result in relatively large traveltime errors when the wavefront curvature is large and the wavefront propagation is diagonal to the grid orientation. In Cartesian coordinates, spherical wavefronts can spend a long time satisfying these two destructive conditions. As a result, implementation of the fast marching method in the Cartesian coordinate, unless the grid is very fine, can result in relatively large errors. Recently, Alkhalifah and Fomel (1997) suggested a spherical coordinate implementation of the fast marching method. In spherical coordinates, wavefronts emanating from a source typically spend less time traveling diagonally with respect to the coordinate system than the case in Cartesian coordinates. As a result, spherical coordinate implementation achieves more accurate traveltimes even for complex models like the Marmousi model, without compromising stability or efficiency.

The SEG/EAGE 3-D velocity model was used to generate 3-D prestack synthetic datasets. These datasets are commonly used to test migration algorithms, especially 3-D prestack Kirchhoff ones. At the center of a 3-D Kirchhoff-based migration is 3-D traveltime computation, and the quality of the migration depends heavily on the accuracy of the traveltime calculation. Thus, the 3-D salt-dome velocity model is useful for testing 3-D traveltime calculation methods, including the fast marching method, which is the main focus here.

In this paper, I will highlight the benefits of executing the fast marching method of traveltime calculation in spherical coordinates. To show these benefits, I will use the SEG/EAGE 3-D salt-dome velocity model. The complexity of the 3-D salt structure provides us with a good measure of the accuracy of spherical coordinate implementation. We will also look into the role that head-waves and other low, but fast, energy arrivals play in traveltime maps.

FAST MARCHING IN SPHERICAL COORDINATES

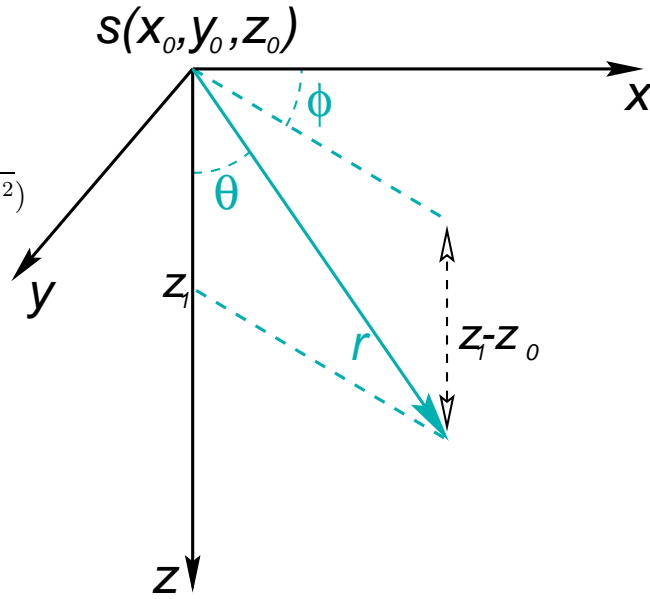
Details of solving the eikonal equation using the fast marching method in Cartesian coordinates can be found in Cao and Greenhalgh (1994) and Sethian (1996), while its application in spherical coordinates can be found in Alkhalifah and Fomel (1997). A summary of the approach, however, is revisited below.

The first-order nature of the fast marching method results in large errors for conventional sparse grid-point configurations. The largest of these errors occur when the curvature of the wavefront is large and the wavefront is traveling diagonally with respect to the orthogonal coordinate system. However, if the wavefront curvature is zero, or the wavefront is parallel to the coordinate system, the fast marching method becomes exact. For waves emanating from a point source, large errors appear in the Cartesian coordinate implementation of the method at angles of 45 degrees from the vertical, especially near the source, where the wavefront curvature is large. Plane

waves, on the other hand, are calculated exactly in the Cartesian-coordinates, because in such coordinates plane waves have no curvature.

In spherical coordinates (Figure 1), waves emanating from a point source are effectively propagated as plane waves on a regular grid. For homogeneous media, these plane waves have fronts that are always parallel to the θ - ϕ plane. As a result, traveltimes calculation using the fast marching approach in spherical coordinates is always exact in homogeneous media (Alkhalifah and Fomel, 1997). Figure 2 shows

Figure 1: A spherical coordinate system given by r , θ , and ϕ . The source, $s(x_0, y_0, z_0)$, is at the origin of the spherical coordinates where $r = 0$. The parameter r ($=\sqrt{(x-x_0)^2+(y-y_0)^2+(z-z_0)^2}$) is the distance from the source to the point of interest along the wavefront, which is also the magnitude of the vector. The parameter ϕ is the angle between the x -axis and the projection of the vector onto the $x-y$ plane. The parameter θ is the angle between the z -axis and the vector along a vertical plane. tariq2-polar-dif [NR]



schematic plots of the progress of this method along a 2-D polar coordinate grid. The source is computed initially and set to zero for all angles θ . When stretched on a regular grid, all points at the surface $r = 0$ are set to zero. These points are inserted in the wavefront array and sorted from minimum traveltimes to maximum. In the case of the source grid point, the sorting step is unnecessary because all traveltimes are equal to zero. The minimum is then extracted, and the traveltimes for neighboring grid points are computed using the following relation:

$$\begin{aligned} \max(D_{ijk}^{-r} t, 0)^2 &+ \min(D_{ijk}^{+r} t, 0)^2 + \\ \max(D_{ijk}^{-\theta} t, 0)^2 &+ \min(D_{ijk}^{+\theta} t, 0)^2 + \\ \max(D_{ijk}^{-\phi} t, 0)^2 &+ \min(D_{ijk}^{+\phi} t, 0)^2 = s_{ijk}^2, \end{aligned} \quad (1)$$

where D_{ijk}^{-r} is the derivative of traveltimes with respect to r at grid point i, j, k , given by

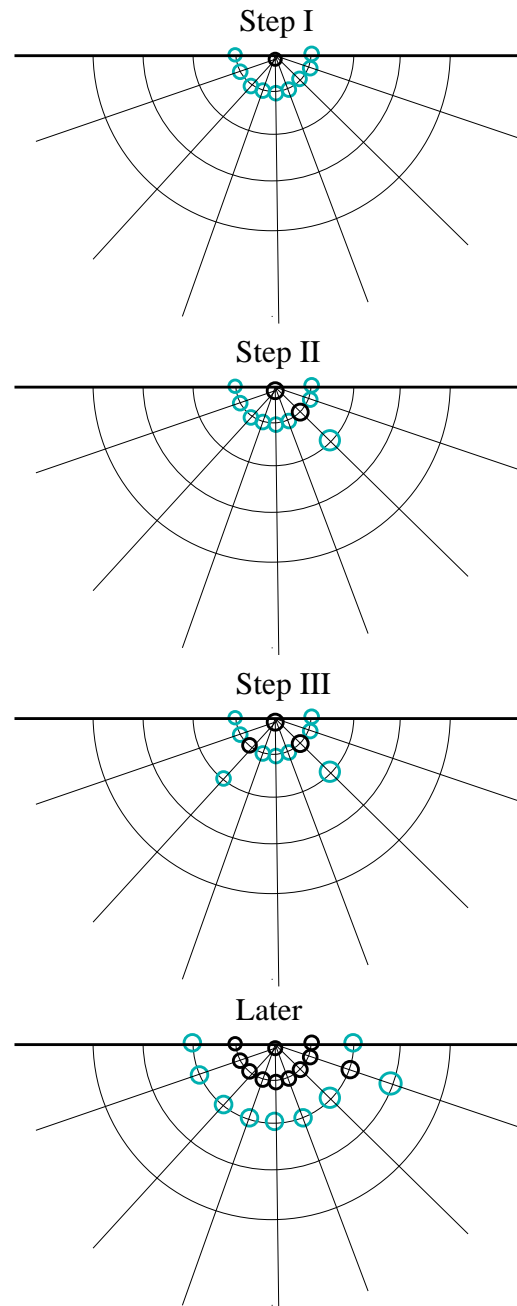
$$D_{ijk}^{-r} t = \frac{t_{i,j,k} - t_{i-1,j,k}}{\Delta r},$$

and

$$D_{ijk}^{+r} t = \frac{t_{i+1,j,k} - t_{i,j,k}}{\Delta r}.$$

Figure 2: The steps taken to implement the fast marching in polar coordinates. Black circles imply computed traveltimes that are set because of their minimum travel-time value along the front. Gray circles constitute the front of the wave, and they are stored in the wavefront heap array and sorted from minimum to maximum travel-time value. The traveltime is schematically given by the size of the circle; the larger the radius, the greater the traveltime. The minimum is always extracted first from the heap array at each step, its traveltime is set (given a black circle), and all surrounding grid points that are not set are computed and put into the heap array. We precede until all grid points are computed and set.

`tariq2-march-pol` [NR]



The D_{ijk}^θ and D_{ijk}^ϕ derivatives are slightly different, given by

$$D_{ijk}^{-\theta} t = \frac{t_{i,j,k} - t_{i,j-1,k}}{r\Delta\theta},$$

$$D_{ijk}^{+\theta} t = \frac{t_{i,j+1,k} - t_{i,j,k}}{r\Delta\theta},$$

$$D_{ijk}^{-\phi} t = \frac{t_{i,j,k} - t_{i,j-1,k}}{r \sin \theta \Delta\phi},$$

and

$$D_{ijk}^{+\phi} t = \frac{t_{i,j+1,k} - t_{i,j,k}}{r \sin \theta \Delta\phi}.$$

The traveltimes t_{ijk} and the slowness s_{ijk} correspond to the grid point that is being updated. Solving for t_{ijk} , the time at a new grid point, requires solving a quadratic equation that has two solutions. We choose the solution that reduces to $t_{ijk} = t_{i-1,j,k} + \frac{\Delta r}{v}$, or $t_{ijk} = t_{i+1,j,k} + \frac{\Delta r}{v}$, when the wavefront travels radially. We do the same for all other unset points surrounding the initial extracted point. Each newly computed grid point is added to the wavefront array, and by using a highly efficient *heap method* the sorting from minimum to maximum traveltimes is done promptly. Then we extract the minimum once again, update all neighboring live grid points, and so on.

Using fast algorithms (heap sorting), the sorting part of the fast marching algorithm can be maintained at a computational cost proportional to $\log N$, where N is the number of grid points in the computational domain. As a result, the cost of the eikonal solver is roughly proportional to $N \log N$. This efficiency feature is maintained in spherical coordinates as well. The cost of transforming traveltimes information from spherical coordinates to Cartesian ones is proportional to N , and thus is less significant.

THE SEG/EAGE SALT DOME MODEL

A joint SEG/EAGE committee was formed in late 1992 specifically for the purpose of creating two 3-D models, which can be used to generate 3-D marine acquisition type datasets. Input for the design of the salt dome model came from 27 geoscientists (experienced in salt tectonics, seismic modeling, and seismic imaging) representing 23 organizations (oil companies, geophysical contractors, and academia). They agreed to base the model on a typical US Gulf Coast salt structure. Special care was taken to ensure that the model was geologically feasible and would be an adequate testing mechanism for seismic imaging algorithms (particularly subsalt).

I will use a program called VIS5D (well known in meteorology circles) to display wavefronts, traveltimes sections, and velocity image maps in 3-D. This program is highly convenient for such tasks, and includes impressive slice and dice capabilities. One limitation of this program is its inability to handle large data sets efficiently. On a Linux machine, the grid size should not exceed 150 grid points in each direction.

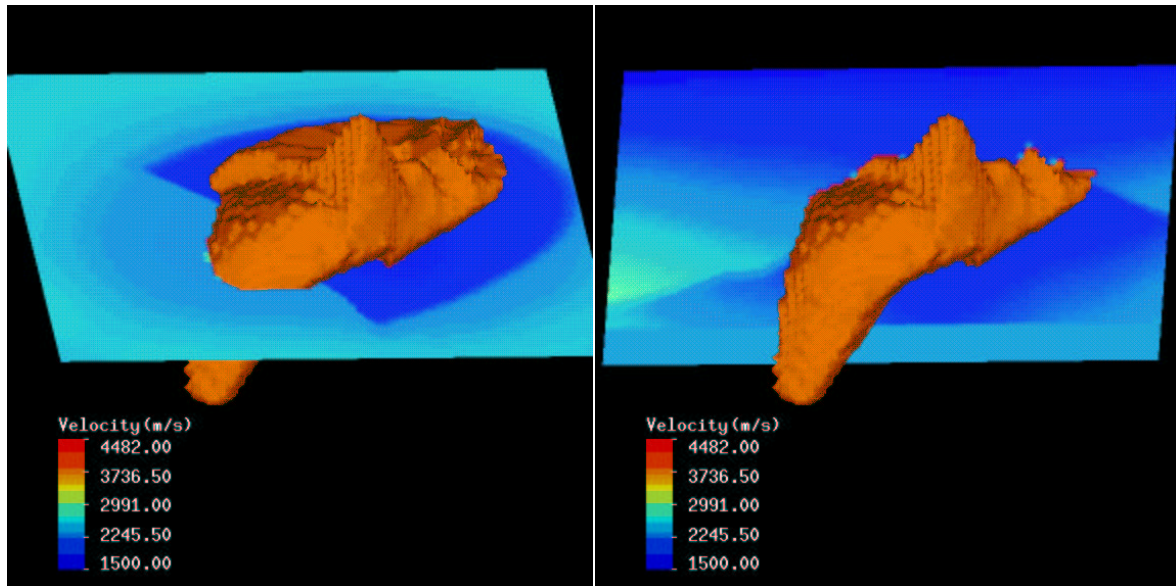


Figure 3: The salt structure displayed from the top. The vertical section (left) is the inline slice through the 3-D salt velocity model and horizontal section (right) is a depth slice through the same velocity model. `tariq2-vel-top` [NR]

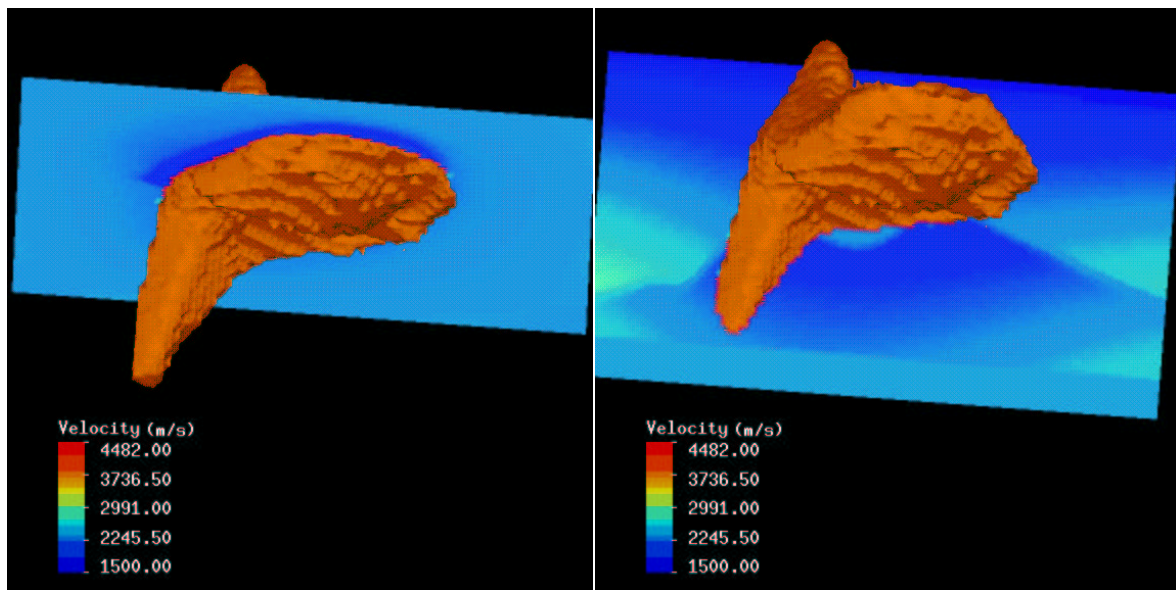


Figure 4: The salt structure displayed from the top (left) and from the bottom (right). The vertical section is the inline slice through the 3-D salt velocity model and horizontal section is a depth slice through the same velocity model. `tariq2-vel-bot` [NR]

Figure 3 shows the salt structure, displayed from the top using VIS5D, embedded onto two slices of the velocity field outside the salt body. The P -wave velocity in the salt is about 4482 m/s. This velocity is much higher than the P -wave velocity in the surrounding sediments, resulting in complicated discontinuities in the P -wavefront (when head-waves are excluded). The high-velocity salt body will also result in head-waves, as we will see later, in the Eikonal solution in areas where such head-waves are the fastest.

Figure 4 shows the salt structure from the bottom with the same two slices displayed in Figure 3 shown here as well. From this view, we can appreciate the complexity of this high velocity salt structure. Proper imaging of the bottom of the salt reflection requires accurate calculation of the traveltimes through the salt body; it also requires using the proper traveltime arrival (typically the most energetic arrival) in areas of multiple arrivals. Unfortunately, finite difference solutions of the eikonal equation provide us only with the fastest arrivals, and not necessarily the most energetic ones.

WAVEFRONTS THROUGH THE SALT BODY

To appreciate the effect that the salt body has on the wavefronts, I will show 3-D plots of the wavefront ISO-surfaces, again using VIS5D, as they penetrate through the salt body. The complex, yet continuous wavefronts include body waves, as well as head-waves.

Figure 5 shows the eight ISO-surface plots of the wavefront at different times along with either a vertical or depth slice of the velocity field. The wavefront expands with time and its shape alters from the typical spherical shape as it penetrates through the salt body. The high salt velocity causes portions of the wavefront to bulge and expand, especially those parts that have penetrated through the salt. The top flanks of this bulge are dominated by the head-wave arrivals, which smoothly connect the portions of the wavefront that penetrated through the salt with those that traveled only through sediments. Clearly, these head-wave flanks have generally low curvature, especially along the vertical plane, indicative of their low amplitude. The low curvature of head-waves in the Cartesian coordinates will translate to high curvature in the polar coordinates. As mentioned above and by Alkhalifah and Fomel (1997), propagating high curvature waves is a weakness of the fast marching approach, especially when propagating diagonally with respect to the coordinate system. As a result, head-waves traveltimes, as we will see later, will include large errors in spherical coordinate implementation of the fast marching method.

The bottom flanks of the wavefronts in Figure 5 also have low curvature on the vertical plane. This portion of the wavefront corresponds to waves that traveled through the high velocity salt, and as a result experienced a lot of spreading. These flanks also replace another, but more important, solution of the Eikonal equation, waves traveling directly from the source, without going through the salt. These

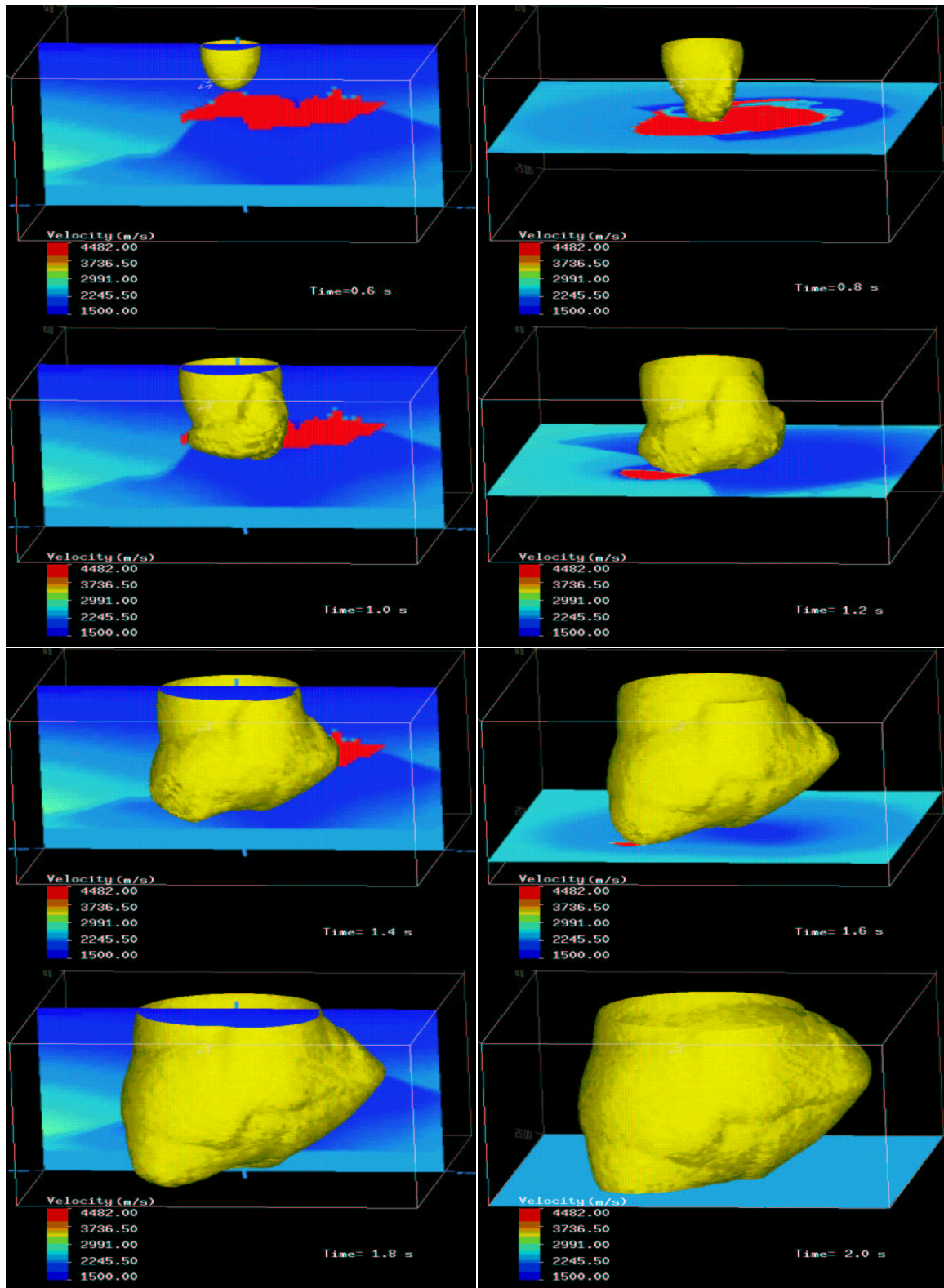


Figure 5: Eight ISO-surface plots of the wavefront at different times, along with the vertical or horizontal slice of the velocity Field. The wavefront corresponds to a wave emanating from the source at the top. The density plots are slices of the velocity field where the salt structure clearly appears in the middle. The vertical velocity slice is kept in the same position, while the horizontal slice of the velocity field is moved along with the wavefront. `tariq2-wavemov` [NR]

waves, however, arrived a little later, and as a result were discluded from the finite-difference solution of eikonal equation solution. Such arrivals and their implications will be discussed further in the head-waves and first arrivals section.

SPHERICAL VERSUS CARTESIAN

To obtain the Eikonal solution using the fast marching method in Cartesian coordinates, I will use Fomel's (1997) program. For the spherical-coordinate implementation, I will use Alkhalifah and Fomel's (1997) program. As a reference solution, I will solve the spherical version of the fast marching method at a much finer grid, since finite -difference solution should converge to the exact solution as the grid size approaches zero. The errors here are exaggerated overall because the grid size used is relatively large. Specifically, we are solving the eikonal at a grid spacing of 40 m in the x-, y-, and vertical z-directions. For spherical coordinates, we use an equivalent spacing that produces results at a comparable time. The reference solution is obtained by using a much finer grid, equivalent to 20 m spacing in the all directions.

Figure 6 shows the errors associated with using the fast marching method in Cartesian coordinates. Specifically, we are looking at the traveltime difference between the coarse-grid Cartesian-coordinate implementation and the fine-grid spherical coordinate implementation. The traveltime errors for such a coarse-grid application are up to 80 ms.

In practice finer grid configurations are often used to solve the eikonal equation at, of coarse, a higher price. The finer grid will result in less errors (for example 8 ms instead of 80 ms). However, the distribution of the errors and the reason for their presence (the first-order nature of the solution) still applies to finer grid implementation. Such errors are inherent in the method and, as Alkhalifah and Fomel (1997) show, when certain conditions are met.

Figure 7 shows the errors associated with using the fast marching method in spherical coordinates. Again, we are looking at the traveltime difference between the coarse-grid spherical-coordinate implementation and the fine-grid spherical coordinate implementation. The traveltime errors for such a coarse-grid application are up to 60 ms, now. Unlike the Cartesian coordinate implementation, most of the errors shown here are associated with low-curvature arrivals, like head-waves. This fact is better demonstrated in Figure 8, where head-waves emanating from the top of the salt are clearly the source of most the errors associated with the spherical coordinate implementation. Luckily, these head-wave arrivals are of low energy, and are generally discarded when it comes to imaging applications. These head-waves, also, mask the more important direct arrival solution. Later, I will show how suggest a method to eliminate such head-wave arrivals, and thus eliminate the source of errors for the spherical coordinate implementation.

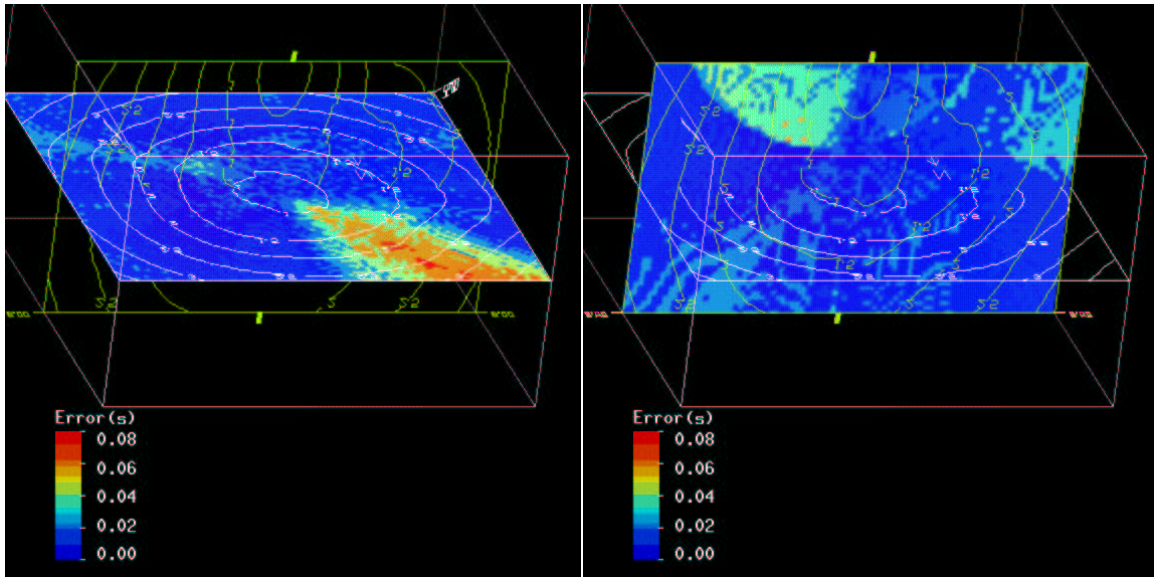


Figure 6: Vertical (left) and horizontal (right) sections of the traveltime errors map that resulted from solving the fast marching method in the Cartesian coordinates. Also displayed are the vertical and horizontal sections of the traveltime contour maps.
 tariq2-errorcar [NR]

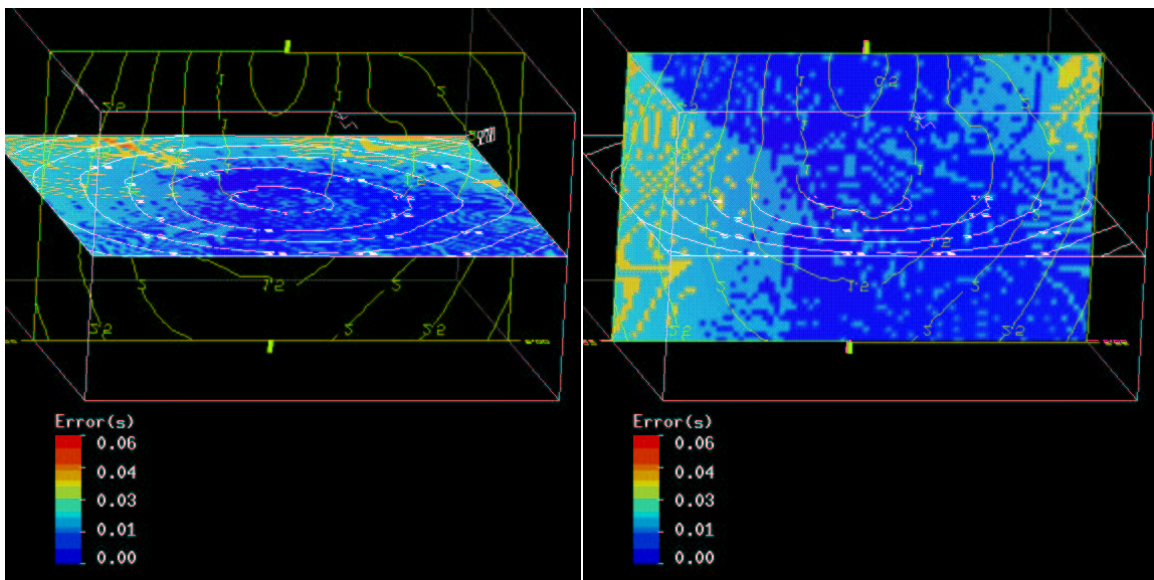


Figure 7: Vertical (left) and horizontal (right) sections of the traveltime errors map that resulted from solving the fast marching method in the Spherical coordinates. Also displayed are the vertical and horizontal sections of the traveltime contour maps.
 tariq2-errorpl [NR]

HEAD-WAVES AND FIRST ARRIVALS

Finite difference solutions of the eikonal equation provide us with continuous wavefront surfaces that correspond to the fastest traveling waves. In the presence of inhomogeneity, such wavefront surfaces might include low-curvature regions corresponding, in some cases, to head-waves that often travel faster than the direct waves. Head-waves are low-energy arrivals that are not useful for imaging applications (Geoltrain and Brac, 1993). The presence of the high velocity salt body in the SEG/EAGE model has intensified the head-waves, and the fast low-energy arrivals problem.

The salt body, because of its very high velocity, acts as a large secondary source that emanates waves from its surface, practically, in all directions. Such waves, typically, have low energy; however, due to their speed through the salt body, they become the fastest arrivals in a big portion of the solution. Most of these waves appear in the solution of the eikonal equation using finite difference methods. Some of these waves correspond to head-waves; others are just low-energy solutions. The energy weakness of such waves is a result of the amount of geometrical spreading they experienced while traveling in the salt body. Typically, the only desired waves emanating through the salt are the ones that travel downward to regions not accessible directly by direct waves.

Figure 9 shows two types of low-energy arrivals. On the left, we see headwaves emanating from the top of the salt structure. These waves travel partly with the salt wave velocity, and thus beat direct arrivals to areas directly above the salt. On the right of Figure 9, we see another arrival that penetrated through the salt body and is thus faster than the direct arrivals. The penetration through the salt body, however, has lowered the energy of such arrivals, causing the wavefront to have low curvature, among other things.

CONCLUSIONS

The fast marching method of solving the eikonal equation is both unconditionally stable and extremely efficient. Both features are well demonstrated on the SEG/EAGE salt-dome model for both the Cartesian and spherical coordinate implementation of the fast marching method. However, the spherical-coordinate version provides more accurate direct-wave traveltimes than the Cartesian coordinate implementation. The only arrivals that suffer in the spherical-coordinate implementation are head-waves, which are not useful for imaging. Head-waves and fast-traveling salt penetrating waves are dominant in the traveltime solutions of the eikonal equation for the salt body model. These arrivals cause problems in imaging data above and beneath the salt in this medium.

Figure 8: Vertical section of the traveltim contour map resulted from solving the Spherical-coordinate fast marching method superimposed on a slice of the error field associated with the spherical-coordinate implementation (like Figure 7. `tariq2-errplhead` [NR]

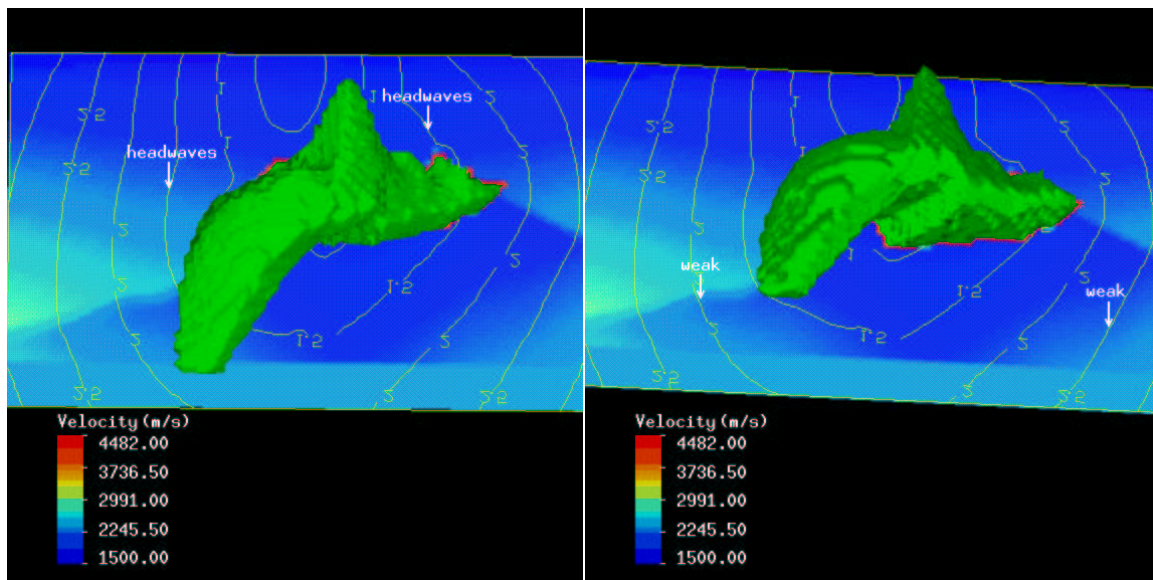
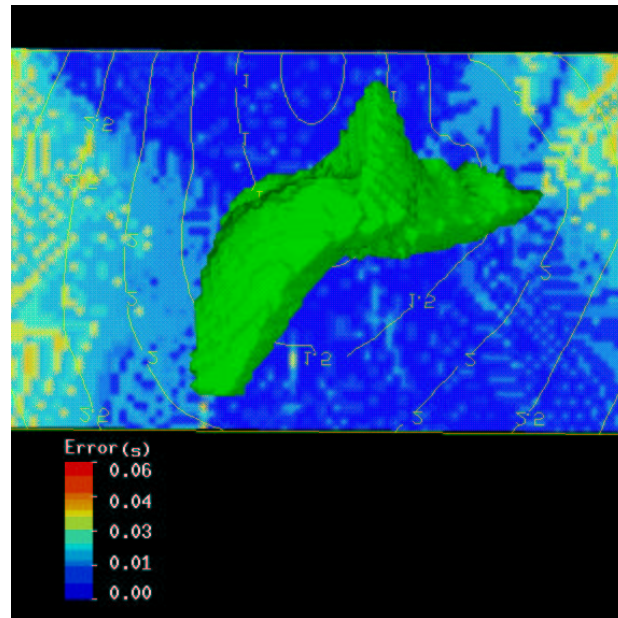


Figure 9: Two-dimensional contour maps of the traveltim with sections of the velocity field displayed in the background and the salt body structure. Left: a semi-top view with the arrow pointing a head-wave. Right: a bottom view with arrows pointing to the portion of the wavefront that traveled through the salt, and thus has weak energy. Both waves, because of their first-arrival nature, have replaced the more useful direct waves. `tariq2-headwaves` [NR]

REFERENCES

- Alkhalifah, T., and Fomel, S., 1997, Implementing the fast marching eikonal solver: Spherical versus cartesian coordinates: *SEP*–**95**, 149–171.
- Cao, S., and Greenhalgh, S. A., 1994, Finite-difference solution of the eikonal equation using an efficient, first-arrival wavefront tracking scheme: *Geophysics*, **59**, no. 4, 632–643.
- Fomel, S., 1997, A variational formulation of the fast marching eikonal solver: *SEP*–**95**, 127–147.
- Qin, F., Luo, Y., Olsen, K. B., Cai, W., and Schuster, G. T., 1992, Finite-difference solution of the eikonal equation along expanding wavefronts: *Geophysics*, **57**, no. 3, 478–487.
- Sethian, J. A., and Popovici, A. M., 1997, Three-dimensional traveltimes computation using the fast marching method: submitted to *Geophysics*.
- Sethian, J. A., 1996, *Level set methods*: Cambridge University Press, New York.